Research Article

Mechanical and tribological characterization of nanostructured HfB_2 films deposited from compound target

Vladimir Buranich[1] · Alexander Pogrebnjak[1] · Piotr Budzynski[2] · Igor Shelest[1] · Adam Prószyński[2] · Dariusz Chocyk[2] · Alexander Goncharov[1] · Andrii Yunda[1]

Received: 5 December 2019 / Accepted: 27 February 2020 / Published online: 5 March 2020

Abstract
Fabrication and development of HfB_2-based nanostructured coatings was investigated. All films were deposited on stainless-steel substrates by RF magnetron sputtering from stochiometric HfB_2 target in argon atmosphere. The aim of this work is to evaluate the effects of the bias potential on the microstructure, mechanical and tribological properties. These parameters strongly depend on the experimental conditions. X-ray diffraction analysis indicated the difference in microstructure: from dense hexagonal structure with (0001) preferred orientation of nanocrystallites to quasi-amorphous with blurred HfB_2 phase peaks. All coatings were measured using nanoindentation (using Berkovich tip), tribology (ball-on-disk) and nano-scratch (friction). Coatings with a thickness of 1–2 μm had a significant dependence of properties on the microstructure: hardness drastically increased from 8 to 45 GPa, H/E ratio and elastic recovery changed respectively: 0.04–0.15 and 0.26–0.72.

Keywords HfB_2 films · RF magnetron sputtering · Mechanical properties · Tribology · Wear

1 Introduction

Various mechanical, tribological and nano-industry applications is always searching for new materials [1]. Transition metal diborides, nitrides and carbides characterized by high hardness, melting point and temperature stability in both bulk and film (nanomaterial) state [2–4]. Physical and chemical properties largely affect the resulting characteristics of the obtained product. Currently, a wide range of vacuum deposition techniques (PVD, CVD) provide an ability to precisely control the deposition process of coatings [4–9].

Titanium, zirconium and hafnium diborides and composites based on their matrix have the highest resistance to thermal influence and oxidizing [10–12]. Films produced at proper conditions can be used for protective coatings in tribo-systems and cutting tools to enhance their durability. The problem of correlation between film structure formation, technological setup subtleties and its influence on the mechanical and tribological characteristics is still unresolved. Similar studies were conducted on the transition metal diborides fabricated by PVD and CVD technologies [13–19]. Obtained coatings were characterized by high shear strength and exceptional wear resistance compared to bulk (standard) values.

Magnetron sputtering is a well-known technology that allows to directly control the interaction of ions with the film growth surface. However, energy distribution of ions in a magnetron discharge is nonequilibrium and highly relies on the potentials caused by the applied power sources and additional bias voltages [20]. The energy density is often described by the laws of collision-less plasma, where the energy caused by induced particles (E_{bi}) is controlled by the difference in the applied potentials, ion/

✉ Vladimir Buranich, hunters325@gmail.com | [1]Sumy State University, 2, Rymskogo-Korsakova Str., Sumy 40007, Ukraine. [2]Lublin University of Technology, Nadbystrzycka 36, 20-618 Lublin, Poland.

SN Applied Sciences (2020) 2:563 | https://doi.org/10.1007/s42452-020-2359-2

electron ratio and the target deposition rate [21, 22]. In the framework of the above, a valuable option is to consider how a positive–negative bias affects the film properties. This question develops the main purpose of this article.

In the present study HfB_2 coatings deposited by RF-magnetron sputtering method onto stainless steel substrates (AISI 321) were investigated. Mechanical, structural and tribological properties of the samples obtained under different conditions has been presented and discussed.

2 Experimental

A planar unbalanced RF-magnetron was used to deposit a hafnium diboride coatings. Detailed explanation of the magnetron sputtering system designed for sputtering of the round targets in Ar^+ atmosphere characterized in [23]. The target material consisted of thermally sintered dense stoichiometric HfB_2 (99.5% purity, 120 mm in diameter). As substrates, mechanically polished AISI 321 stainless steel plates (20 × 10 × 3 mm) with a surface roughness of R_a = 0.25 µm were used. All substrates were ultrasonically cleaned consecutively in acetone and ethanol and rinsed with de-ionized water for 10 min.

Deposition was carried out at constant power P = 500 W, working pressure p = 0.65 Pa. Substrate-target distance (d_{s-t}) was 100 mm and the substrate temperature kept at 500 ± 50 °C (through an increase in the electron/ion mobility by biasing). Bias potential U_S varied from − 50 to 50 V (with 25 V one step) to evaluate difference in the internal structure of coatings deposited at different conditions. The film deposition time lasted 60 min for all samples, and the Ar flow rate during deposition was 10 sccm.

Substrate surface roughness and film thicknesses was measured by the using the MII-4 multiple-beam optical profilometer/interferometer with monochromatic light source. Surface roughness and film thickness values also refined from the microscopical studies performed on SEM–106 (Selmi, Ukraine) at 30 kV accelerating voltage.

X-ray diffraction analysis was performed on DRON-3 M diffractometer in Cu-Kα radiation (40 kV, 20 mA) at Bragg–Brentano beam focusing (θ–2θ geometry). Grain sizes normal to the film plane estimated from the broadening of the dominant (0001) diffraction peak using the well-known Scherrer relationship [24].

Hardness and Young's modulus measured by the nanoindentation method using the Ultra-Nano Hardness Tester (UNHT) from CSM Instruments equipped with a Berkovich tip. Numerical calculations of mechanical properties were performed according to the Oliver and Pharr method [25]. Films hardness calculated using the following equations:

$$H = \frac{P_{max}}{A}, \tag{1}$$

where P_{max} is the maximum load applied to the surface, A is the contact area of the indenter.

$$A = k_1 h_c^2 + k_2 h_c, \tag{2}$$

where k_1 and k_2 are constants defined by the geometry of indenter.

$$h_c = h_{max} - 0.75 P_{max} \left(\frac{dh}{dP}\right)_{P_{max}}, \tag{3}$$

where h_{max} is the maximum depth of the indenter penetration.

Friction and wear tests were performed using Anton Paar pin/ball-on-disc Nano Tribometer (NTR_2). The tribological behavior was analyzed in dry conditions. One rotation of the sample corresponded to one cycle. The air temperature was 22 °C at a relative humidity of 30–50% and an atmospheric pressure of 1000 hPa. A tungsten carbide (WC) ball with a diameter of φ = 1.0 mm with 300 mN load was used as a counter-body. The cross-sectional area of the track made by the WC ball was a measure of wear. Wear trace of each sample was measured using the Form Talysurf Intra Taylor–Hobson profile measurement gauge. Measurements of the obtained profilograms enabled determination of the average wear of wear trace. The wear was defined as the mean surface of the cross section of the contact between the sample (steel substrate + film area) and the counter-sample (WC).

The friction coefficient was determined based on a scratch test carried out on a Nanoscratch Tester (NST) (CSM instruments) equipped with a spherical diamond indenter. The measurments were made with a constant load of 50 mN, with a scratch length of 0.8 mm, at a rate of 0.12 mm/min. The residual penetration depth obtained by performing the additional scratch scans before and after the primary scratch. Therefore, each measurement (one scratch) consisted of three measurements: (1) the so-called pre-scan, the purpose of which was to determine the height and the surface profile before scratch, (2) primary scratching with a given length and force, and (3) the post-scan, which was supposed to be used for the evaluation of the height and the surface profile after scratch. The residual depth calculated as the difference in height of the sample before and after scratching. The friction coefficient calculations were carried out according to the method described in [26].

3 Results and discussion

Figure 1 shows low-magnification SEM images revealing the typical microstructure of HfB_2 coatings. Under all of the applied deposition conditions, the obtained HfB_2 films had uniformly fine grain structure in film thickness over the entire stainless-steel substrate.

The cross section images of the coatings show a densely packed structure that is suitable for the transition zone on the Thorntons model [27] ($T_S/T_M = 0.2–0.5$). Via constant heating, the Ar flow rate, and RF-source power of 500 W obtained films exhibit an almost identical morphology. In addition, coatings deposited at negative bias potentials had a wavy surface and were rather uniformly distributed across the substrate. According to the literature [28, 29] packing density increases with smoothering the surface. That consequence of the nucleation sites formation at more intense argon ion bombardment.

HfB_2 films thickness as a function of applied DC bias voltage is shown in Fig. 2 for a fixed deposition time of 1 h. In the range of bias potential values going from 0 V to negative and positive voltages the film thickness decreases. A maximum thickness of 1650 nm is obtained for substrate bias at 0 V, while minimum thickness was ~ 1150 nm for − 50 V. The difference in the film thickness as a function of applied bias can be related to the operating film growth and sub-surface processes initiated by the incoming particles [30]. Plasma and floating potentials also related to processes occurring on the surface [22], differences in ion/electron ratios and magnetic field of magnetron itself [21]. This is, however, beyond the scope of this paper and require more rigorous studies.

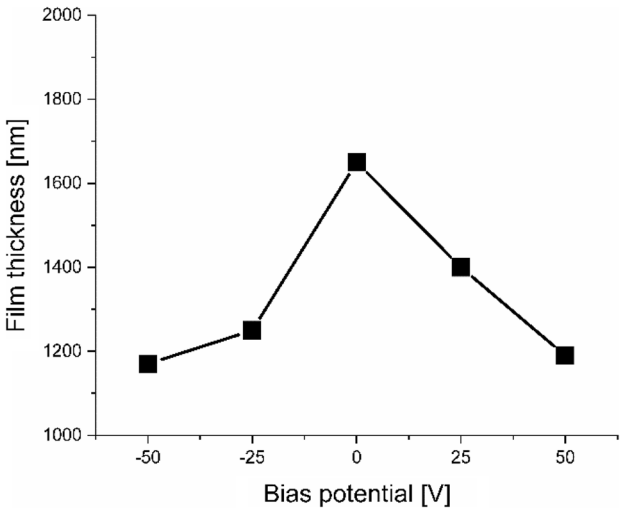

Fig. 2 Average film thickness as the function of the applied (DC) bias voltage (optical profilometry data)

The X-ray diffraction analysis (Fig. 3) clearly shows the presence of HfB_2 phase (structural type AlB_2, space group P6/mmm). Diffraction data were indexed along the ICSD reference cards 30422, 53022 and 103497 for HfB_2, Hf and

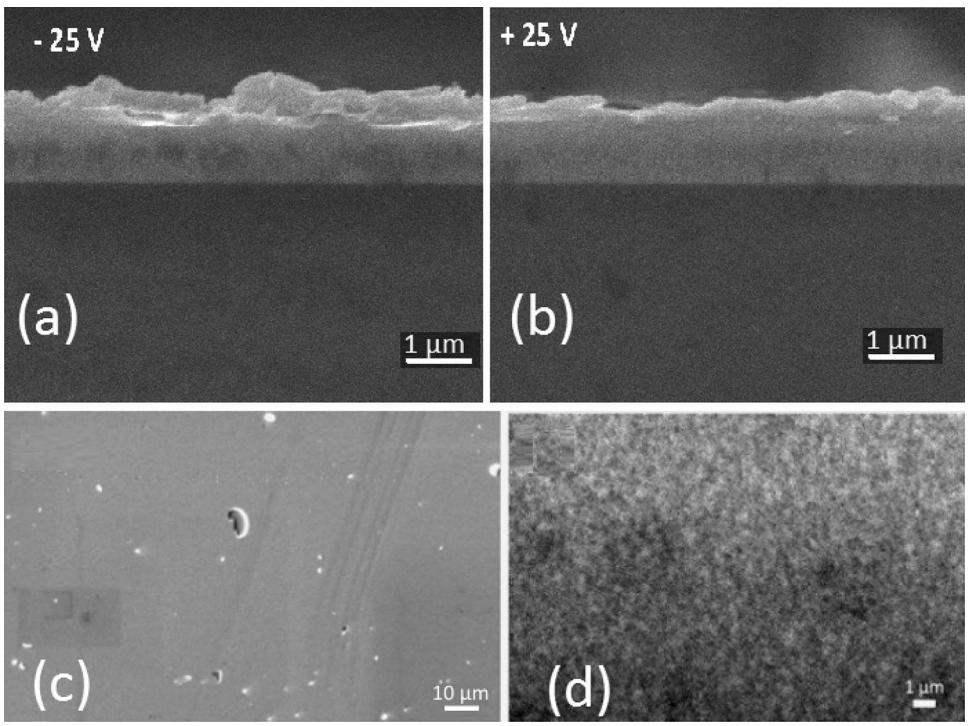

Fig. 1 SEM micrographs visualization of the film: cross section (**a**, **b**), surface morphology (**c**, **d**). This image corresponds to the samples coated at $U_S = +25$ V and $U_S = -25$ V

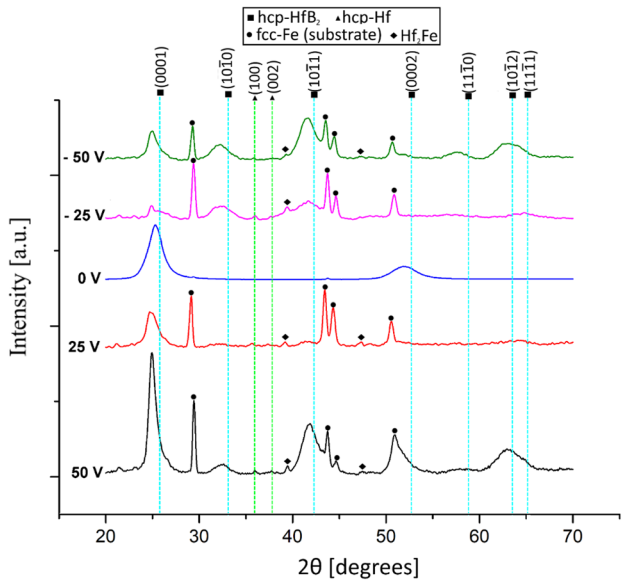

Fig. 3 XRD patterns of the as-deposited on the stainless-steel substrates HfB_2 coatings deposited at different bias potential

Hf_2Fe, respectively. All major peaks (0001), (10$\bar{1}$0), (101$\bar{1}$), (0002) and (10$\bar{1}$2) related to this phase was observed. Some low-intensity hcp-Hf diffraction reflections is visible. The possible presence of a thick (10–50 nm) epitaxial Hf-interlayer may cause Hf peaks at diffraction pattern. Assumption of such effect supposed because by (0001) plane of metal atoms in both Hf and HfB_2 are virtually identical in geometric structure [31]. Broadness and high shift of diffraction peaks in comparison with bulk Hf reveals intrinsic stresses during relaxation and high degree of disorder in crystal lattice of this layer. No crystalline boron phase was detected (ICSD 56992).

As-deposited coatings exhibit comperehensive macrostrain which indicated from HfB_2 diffraction peaks shifted to lower angles. The lattice parameter *c* drastically increased. Basically lattice strain in such type of material associated with B–B bonding along the a axis. B-rich tissues can led to enhance in hardness as was reported for TiB_2 and ZrB_2 films [14, 17].

Iron borides may be presented in the coating, but it is impossible to resolve these peaks due to the large overlay with hafnium structure peaks and the nature of low-intensity FeB binary systems. Epitaxial growth may be a possible case, since the most intensive peak of the FeB phase is also the hcp (0001) [32].

The Hf_2Fe peaks point disordered thin clusters of tissue-free Hf-Fe bonds from the surface interlayer of pure Hf. According to the phase diagram, the Hf_2Fe phase is most likely to form when the percentage of Hf is below 60%, which is achieved by huge abundance of boron only [33].

As films were growing on a preheated substrate, they show hexagonal crystal phase and increased (0001) intensity at mostly all biases. At grounded substrate ($U_S = 0$ V), we observe crystalline phase highly oriented perpendicular to the (0001) plane orientation, all peaks except substrate peaks and (0002) reflection are blurred to noise due effect of texture. At positive substrate bias of 25 V (10$\bar{1}$0), (10$\bar{1}$1), (11$\bar{1}$1), (10$\bar{1}$2) diffraction peaks appeared and, as a result, the intensity of the (0001) peak decreased. Increasing the bias potential up to 50 V leads to the formation of nanostructured films with more pronounced (0001) orientation and visible (10$\bar{1}$0), (10$\bar{1}$1), (10$\bar{1}$2), and (11$\bar{1}$1) diffraction peaks. At increased negative U_S, moving ions can transfer more momentum to the coating surface. This process leads to a fast diffusion characterized by the disorder of (0001) orientation and crystal lattice distortion. Adatoms rearrange in other energetically favorable planes that supports with larger lattice parameters shift regarding to pristine (bulk state). An amorphous or random-oriented nanocrystalline structure formed when negative substrate bias $U_S = -25$ V was applied. Large peak asymmetry is visible along with grain size granulation up to 3 nm. Patterns of films deposited under $U_S = -50$ V displays hexagonal phase with a (10$\bar{1}$1) orientation and increase in the grain size up to 9 nm.

Since we have different values of the grain sizes it is also important to define the impact of their orientation along the diffraction planes. The texture coefficient (T_{hkil}), which indicates the maximum preferred orientation of the films along the diffraction plane, means that the increase in the preferred orientation is associated with the increase in the number of grains along that plane. In order to investigate the texture development as a function of bias voltage variation, the texture coefficients of the HfB_2 T_{hkil} were calculated from their respective XRD peaks with the following formula [13]:

$$T_{hkil} = \frac{I_{hkil}}{\sum_{i=1}^{n} I_{hkil}}, \tag{4}$$

where I_{hkil} represents the intensity of all major HfB_2 phase orientations. The texture coefficients variation as a function of bias voltage is presented in Fig. 4.

Films grown under weak ion-irradiation under null and positive potentials contain a predominant (0001) texture. Whereas at negative biases (0001) texture coefficient trend exhibited a decrease against (10$\bar{1}$1) orientation, which is closer to the single-crystal state. The (10$\bar{1}$1) reflection dominance can be explained as a consequence of an increase in the packing ratio (*c*/*a*) at a negative bias. The observed discrepancy between the values of the texture coefficient and grain size can be expressed in the fact that, in the nanostructured state, the size of nanocrystallites

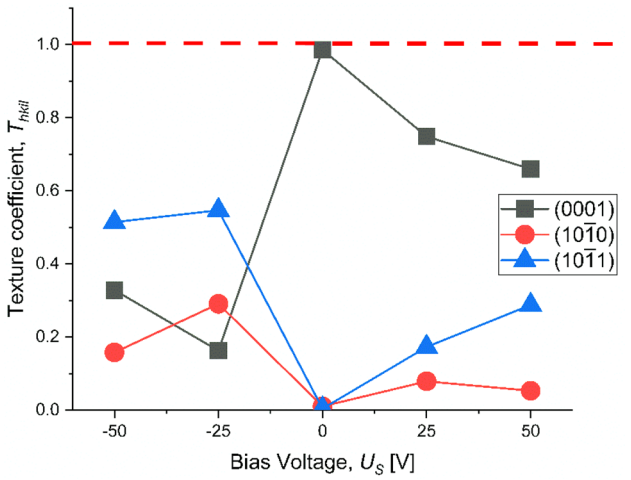

Fig. 4 Texture coefficient of the as-deposited HfB2 films relative to bias voltages

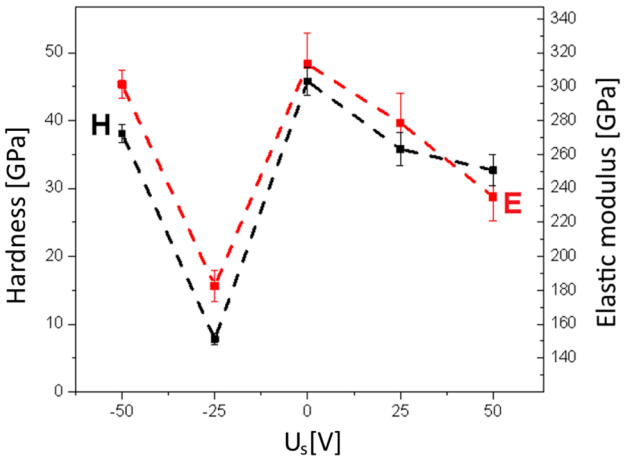

Fig. 6 The dependence of the indentation hardness and elastic modulus on applied bias voltage in the studied HfB_2 coatings

affects the microstructure, as well as the density of grain boundaries [34].

Studies devoted to the mechanical properties' investigations of the DC-magnetron sputtered Ti-B coatings [35–37], mentioned that (0001) oriented transition metal diboride coatings provide improved mechanical properties: $H = 40–50$ GPa and $W > 80\%$. The results of the mechanical test are summarized in Figs. 5 and 6. Figure 5 shows the load–displacement curves of the HfB_2 samples. Calculated data presented against structural XRD studies (Table 1). We observe a non-linear distribution on the Fig. 6. The highest values, 46 GPa and ~360 GPa, respectively, were obtained for the coating deposited at the grounded substrate, whereas the lowest values (8 GPa and 175 GPa, respectively) for the coating at the $U_S = -25$ V.

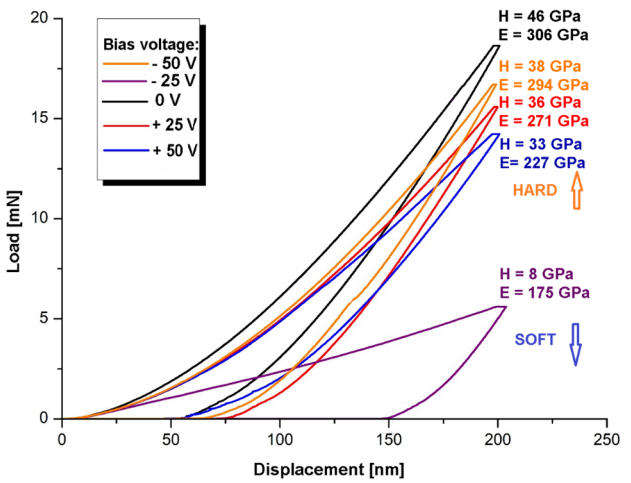

Fig. 5 Load–displacement curves for HfB_2 coatings deposited at different bias potential

Presuming that sizes of the grains of all sample have the same order 1–10 nm and huge lattice distortion of both lattice parameters this indicates a huge predominance of main structural defects dislocations and vacancies. In case of sample sputtered at $U_S = -25$ V structure becomes quasi-amorphous and dislocations tend to coalescence. But at bias potential $U_S = 0$ V with intensive (0001) oriented texture the energy of condensed particles is enough to form from a Hf-B amorphous matrix a dense superhard coating.

To investigate the wear resistance, the conditions of development-type coatings (wear depth exceed 10 µm) was applied. In these conditions coefficient of friction (COF) mostly showed the influence of the steel substrate. The measured COF values exceeds 0.6 (steel) after 200 cycles and rise to the 3–4 below 2000 with further linear curvature of the slope. These data were not informative and were used only to characterize wear resistance. Wear values taken as summarized wear worn of the coated surface. The constructed profilograms of wear tracks are shown in Fig. 7.

Samples were measured for abrasive wear after 10,000 cycles. Due to flaking of a counter-body, coatings applied at $U_S = 50$ V and -25 V were measured at 2000 cycles. Figure 7 shows that their volume loss is much bigger than wear of other samples. As can be be seen samples with (0001) oriented grain structure shows the highest wear resistance at the macro scale. The discrepancy between the values of the depth and width of wear is apparently related to the features of the surface, as well as to different growth mechanism stimulation. Due to the difference in the mobility of ions and electrons at different bias potentials, the surface energy for crystalline structure formation may be too large or vice versa.

Table 1 Comparison of the microstructural and mechanical characteristics of HfB_2 coatings

U_S (V)	a (Å) 3.1425*	c (Å) 3.4760*	D (nm)	H (Gpa)	E (Gpa)	H/E	H^3/E^2	W (%)
− 50	3.1926	3.5358	8.8	38.1 ± 1.3	293.7 ± 8.2	0.13	0.64	66.7
− 25	3.1817	3.5180	3.6	7.8 ± 0.8	175.0 ± 9.3	0.04	0.02	26.3
0	$d_{00.1}$ = 3.5133		9.1	45.8 ± 2.1	305.6 ± 18.6	0.15	1.03	72.1
25	3.2018	3.5390	6.5	35.8 ± 2.4	271.0 ± 17.2	0.13	0.62	62.2
50	3.1646	3.5420	10.8	32.7 ± 2.3	227.4 ± 14.2	0.14	0.68	72.3

Notable changes based on the internal structure of the presence of impurity phases such as Hf, Hf_2Fe, Fe_2B on the hardness and wear characteristics had not seen. Few researchers [2, 6, 9] suggested that hardness of transition metal diboride coatings correlates well with their crystal structure. Decrease in intensity of X-ray reflection lines and increase of thier broadening results in increase of hardness. In contrary to this impurity phases lead to disoriented small grains distribution and decrease of the (0001) orientation.

According to the theory of material wear, hardness is the main characteristic that determines the surface wear resistance [38–40]. To assess the resistance of materials to elastic fracture strain, the ratio of hardness to elastic modulus (H/E) [41, 42] is inversely proportional to the material plasticity index, and to estimate the resistance of the material to plastic deformation the H^3/E^2 parameter is used. In order to increase the resistance to elastic deformation of fracture and reduce plastic deformation, the material should have high hardness with low elasticity modulus [43]. Hafnium diboride coatings with an adaptive structure are quite promising to use as material with high hardness and reduced elastic modulus. Formation of the nanocrystalline structure in thin layer leads to an increase in the hardness and a decrease in the elastic modulus of surface. In addition, to estimate the ability of the material to resist plastic deformation, the H^3/E^2 parameter from the nanoindentation data was used [44].

To get information about surface friction, a nanotribological test was conducted. The nanoscratch tests was performed three times with the same force of 50 mN and a length of 0.8 mm for each sample. The dependence of the friction force and residual depth on the path of scratch-tester tip is shown in Fig. 8. The evolution of the friction coefficient was defined from 200 dots as a ratio between normal force (50 mN) to normalized value of the friction force [45].

Overall results of the tribological assessment are presented in Table 2. Measured wear resistance correlates well with the hardness of the coating. In order to complete the whole picture, it is necessary to discuss the relations of the Young's modulus and hardness, as the main parameters determining the ability of the material to resist plastic end elastic deformation. A higher H^3/E^2 ratio evaluate the ability of a material to dissipate energy during plastic deformation (e.g. load). With high H^3/E^2 coatings gain increased wear resistance. In most cases H^3/E^2 determine the tribological parameters. Nevertheless, taking into account the presence of huge fluctuations caused by surface irregularities in our specimen, the values of friction should be considered in terms below classic theory of friction [38].

Friction force–displacement dependence had a "stick–slip" shape. This type of slippage observed in tribological systems with kinetic friction less than the static friction force. Rabinovich description of the "stick–slip" model [38] suggests that two rough macroscopic surfaces stick through their microscopic irregularities of characteristic length. In our experiment, we observed the complex of irregularities based on the initial roughness of steel substrate and damage caused by particle elastic collisions. During shear, each surface must first crawl the size of the contacting joints, after which the surfaces continue to slide, but with less (kinetic) friction force than the original (static) value. Friction force remains high during stick–slip. However, as the surfaces shifted by a characteristic distance, the friction quickly drops to a kinetic value.

4 Conclusion

During this study a HfB_2 coatings with thickness of 1–2 µm was fabricated on the surface of stainless-steel substrates by means of RF magnetron sputtering for 1 h in argon atmosphere. All working parameters except applied (DC) bias voltage kept constant, to investigate the impact of biasing on the structure and properties of deposited coatings.

Microstructure of obtained films depended on the bias potential which affected the surface during growth. Structure of the obtained films varied from X-ray amorphous with low intensity of HfB_2 phase to nanostructured with dominating (0001) orientation, grain sizes changed from 3 to 11 nm accordingly.

Mechanical and tribological testing of samples indicate the effect of microstructure on acquired properties: film deposited at $U_S = 0$ V show highest values of hardness ($H = 45$ GPa), Youngs modulus ($E = 306$ GPa) and

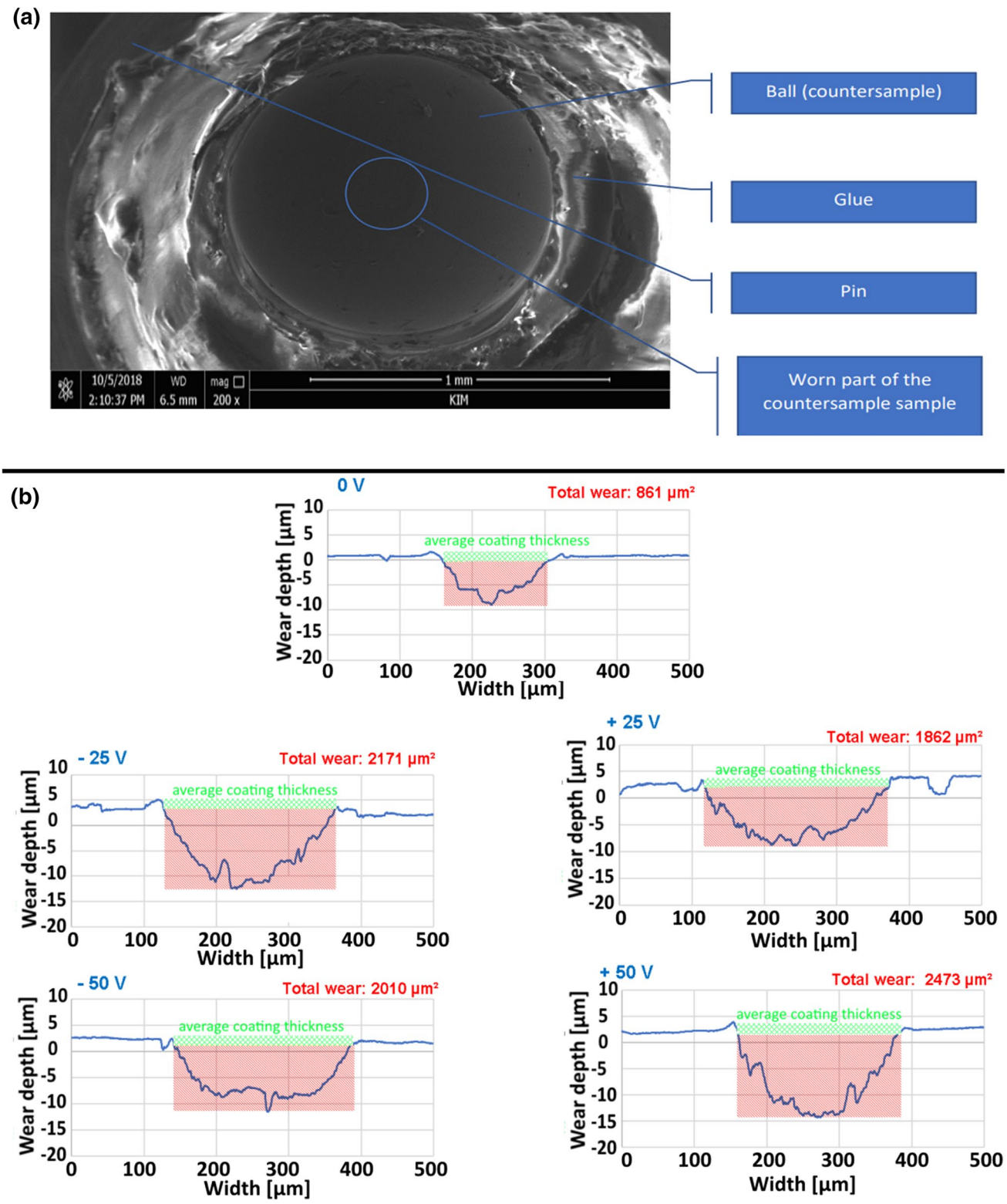

Fig. 7 Representative procedure of wear measurement (**a**), experimental profilograms of a track worn by the ball on the HfB_2 samples obtained under different substrate biases (**b**)

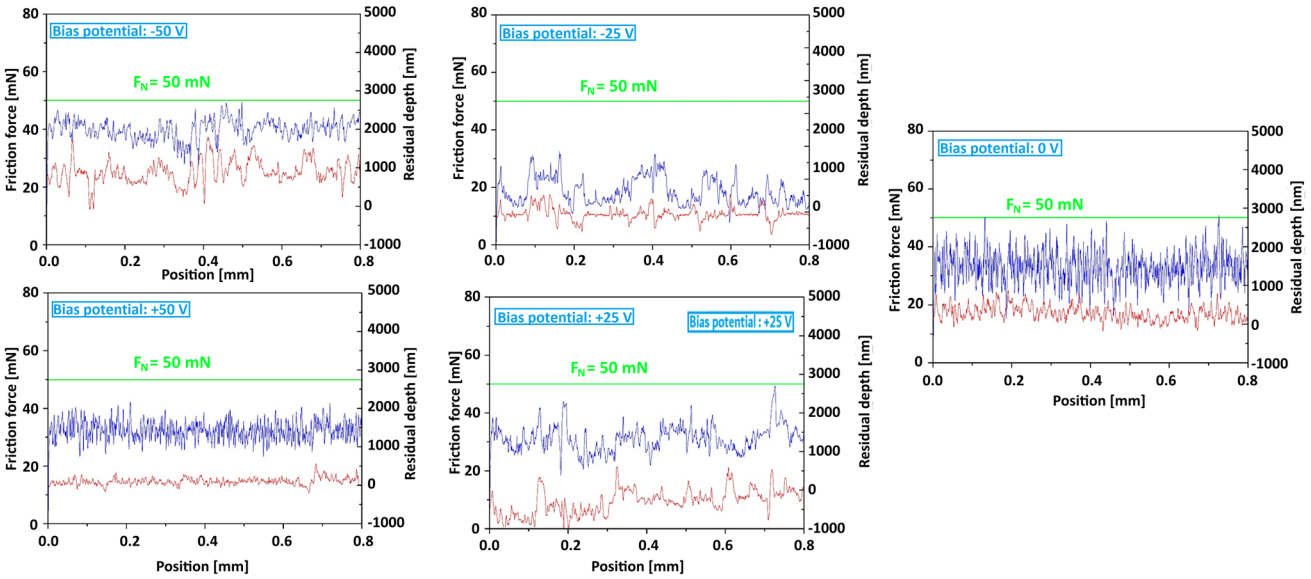

Fig. 8 Dependence of normal force (green line), friction force (blue line) and residual depth (red line) against the length position for HfB2 samples

Table 2 Tribological characteristics of HfB_2 coatings (H and H^3/E^2 derived to compare)

Bias potential (U_S)	<H> (GPa)	H^3/E^2	Mean wear (μm^2)	Standard deviation	Mean wear track depth (μm)	Friction coefficient (μ)	Friction fluctuation
− 50 V	38	0.64	2111.95	244.32	12.21	0.776	Notable
− 25 V	8	0.02	Exceed 2176.33 μm^2		–	0.398	Notable
0 V	45	1.03	871.95	101.54	9.34	0.652	Significant
+ 25 V	36	0.62	1860.86	155.01	11.47	0.622	Notable
+ 50 V	33	0.68	2450.87	160.01	16.49	0.624	Significant

Elastic modulus ($W = 72\%$). The total loss of volume shows a strong effect of hardness on the ability of the film against abrasion. On the other hand, not only hardness and H/E ratio determine coatings with low wear resistance. Moreover, conducted experiments show efficiency of investigation of the growth and nucleation, as well as texture evolution, that takes place in case of dense hexagonal close-packed lattice.

This suggests a further promising use of magnetron sputtered HfB_2 coatings as a protective layer in tribomechanical applications. However, development of coatings with controled coefficient of friction and knowledge of its effect on the structure evolution require further more devoted studies.

Compliance with ethical standards

Conflict of interest On behalf of all authors, the corresponding author states that there is no conflict of interest.

References

1. Olafusi OS, Sadiku ER, Snyman J et al (2019) Application of nanotechnology in concrete and supplementary cementitious materials: a review for sustainable construction. SN Appl Sci 1:580. https://doi.org/10.1007/s42452-019-0600-7
2. Musil J (2000) Hard and superhard nanocomposite coatings. Surf Coat Technol 125:322–330. https://doi.org/10.1016/S0257-8972(99)00586-1
3. Xie C, Zhang Q, Zakaryan HA, Wan H, Liu N, Kvashnin A, Oganov A (2019) Stable and hard hafnium borides: a first-principles study. J Appl Phys 125:205109. https://doi.org/10.1063/1.5092370
4. Pogrebnjak AD, Beresnev VM, Bondar OV, Postolnyi BO, Zaleski K, Coy E, Jurga S, Lisovenko MO, Konarski P, Rebouta L, Araujo JP (2017) Superhard CrN/MoN coatings with multilayer architecture. Mater Des 153:47–59. https://doi.org/10.1016/j.matdes.2018.05.001
5. Cobbinah PV, Matizamhuka WR (2019) The effect of SiC content on the tribocorrosion performance of spark plasma sintered Al–SiC nanocomposites. SN Appl Sci 1:1679. https://doi.org/10.1007/s42452-019-1770-z
6. Kunc F, Musil J, Mayrhofer PH, Mitterer C (2003) Low-stress superhard Ti-B films prepared by magnetron sputtering. Surf

Coat Technol 174:744–753. https://doi.org/10.1016/S0257-8972(03)00425-0
7. Pogrebnjak D, Yakushchenko IV, Bondar OV, Beresnev VM, Oyoshi K, Ivasishin OM, Amekura H, Takeda Y, Opielak M, Kozak C (2016) Irradiation resistance, microstructure and mechanical properties of nanostructured (TiZrHfVNbTa)N coatings. J Alloys Compd 679:155–163. https://doi.org/10.1016/j.jallcom.2016.04.064
8. Smyrnova KV, Pogrebnjak AD, Beresnev VM, Litovchenko SV, Borba-Pogrebnjak SO, Manokhin AS, Klimenko SA, Zhollybekov B, Kupchishin AI, Kravchenko YO, Bondar OV (2018) Microstructure and physical–mechanical properties of (TiAlSiY)N nanostructured coatings under different energy conditions. Met Mater Int 24:1024–1035. https://doi.org/10.1007/s12540-018-0110-y
9. Mayrhofer PH, Mitterer C, Wen JG, Greene JE, Petrov I (2005) Self-organized nanocolumnar structure in superhard TiB2 thin films. Appl Phys Lett 86:131909. https://doi.org/10.1063/1.1887824
10. Cheneke S, Karunakar D (2019) The effect of solution treatment on aging behavior and mechanical properties of AA2024-TiB2 composite synthesized by semi-solid casting. SN Appl Sci 1:1501. https://doi.org/10.1007/s42452-019-1531-z
11. Peçanha L, Monteiro S, Tomaz Í, Mendes M, Ramalho A, Simonassi N, Braga FJ (2018) Characterization of TiB2-AlN composites for application as cutting tool. Mater Res Technol 7:550–553. https://doi.org/10.1016/j.jmrt.2018.07.010
12. Moghanlou FS, Vajdi M, Sha J, Motallebzadeh A, Shokouhimehr M, Asl MS (2019) A numerical approach to the heat transfer in monolithic and SiC reinforced HfB2, ZrB2 and TiB2 ceramic cutting tools. Ceram Int 45:15892–15897. https://doi.org/10.1016/j.ceramint.2019.05.095
13. Zhang TF, Gan B, Park S, Wang QM, Kim KH (2014) Influence of negative bias voltage and deposition temperature on microstructure and properties of superhard TiB2 coatings deposited by high power impulse magnetron sputtering. Surf Coat Technol 253:115–122. https://doi.org/10.1016/j.surfcoat.2014.05.023
14. Silva FJG, Casais RCB, Martinho RP, Baptista APM (2012) Mechanical and tribological characterization of TiB2 thin films. J Nanosci Nanotechnol 12:9187–9194. https://doi.org/10.1166/jnn.2012.6759
15. Chatterjee A, Jayaraman S, Gerbi JE, Kumar N, Abelson JR, Bellon P, Polycarpou AA, Chevalier JP (2006) Tribological behavior of hafnium diboride thin films. Surf Coat Technol 201:4317–4322. https://doi.org/10.1016/j.surfcoat.2006.08.086
16. Chowdhury S, Polychronopoulou K, Cloud A, Abelson JR, Polycarpou AA (2015) Nanomechanical and nanotribological behaviors of hafnium boride thin films. Thin Solid Films 595:84–91. https://doi.org/10.1016/j.tsf.2015.10.030
17. Chen WC, Lee CT, Su J, Chen HP (2019) The effects of annealing temperature on the structural properties of ZrB2 films deposited via pulsed DC magnetron sputtering. Coatings 9:253–263. https://doi.org/10.3390/coatings9040253
18. Tengdelius L, Broitman E, Eriksson J, Lu F, Birch J, Nyberg T, Hultman L, Högberg H (2016) Hard and elastic epitaxial ZrB2 thin films on Al2O3(0001) substrates deposited by magnetron sputtering from a ZrB2 compound target. Acta Mater 111:166–172. https://doi.org/10.1016/j.actamat.2016.03.064
19. Akçamlı N, Ağaoğulları D, Balcı Ö, Öveçoğlu ML, Duman İ (2016) Synthesis of HfB2 powders by mechanically activated borothermal reduction of HfCl4. Ceram Int 42:3797–3807. https://doi.org/10.1016/j.ceramint.2015.11.041
20. Haase F, Lundin D, Bornholdt S, Kersten H (2015) On the impact of electron temperature in magnetron sputtering benchmarked with energy flux measurements. Contrib Plasma Phys 55:701–713. https://doi.org/10.1002/ctpp.201510020
21. Zhou J, Wu Z, Liu Z (2008) Influence and determinative factors of ion-to-atom arrival ratio in unbalanced magnetron sputtering systems. J Univ Sci Technol B 15:775–781. https://doi.org/10.1016/S1005-8850(08)60286-8
22. Musil J, Jaroš M (2017) Plasma and floating potentials in magnetron discharges. J Vac Sci Technol A 35:060605. https://doi.org/10.1116/1.4992054
23. Goncharov AA, Yunda AN, Buranich VV, Shelest IV, Loboda VB (2018) Effect of RF-magnetron sputtering parameters on the structure of hafnium diboride films. J Nano-Electron Phys 10:03002. https://doi.org/10.21272/jnep.10(3).03002
24. Patterson AL (1939) The scherrer formula for X-ray particle size determination. Phys Rev 56:978. https://doi.org/10.1103/PhysRev.56.978
25. Oliver WC, Pharr GM (1992) An improved technique for determining hardness and elastic modulus using load and displacement sensing indentation experiments. J Mater Res 7:1564–1583. https://doi.org/10.1557/JMR.1992.1564
26. Broitman E (2015) Novel method for in-situ and simultaneous nanofriction and nanowear characterization of materials. J Vac Sci Technol A 33:043201. https://doi.org/10.1116/1.4921584
27. Thornton J (1974) Influence of apparatus geometry and deposition conditions on the structure and topography of thick sputtered coating. J Vac Sci Technol 11:666–670
28. Zhang Y, Li Q, Tian Z, Qin X, Yung F (2020) Gas-sensing properties of ITO materials with different morphologies prepared by sputtering. SN Appl Sci 2:264. https://doi.org/10.1007/s42452-020-2050-7
29. Dai W, Zhang T, Yang J, Sun R (2008) Morphological analysis of TiB2 thin film prepared by rf magnetron sputtering. J Vac Sci Technol A 26:610–615. https://doi.org/10.1116/1.2943642
30. Goncharov AA, Zykov AV, Yunda AN, Shelest IV, Buranich VV (2020) Effect of energy factors on the structure, and substructure characteristics of hafnium diboride films deposited by rf-magnetron sputtering. Metallofizika i Noveishie Tekhnologii (Metallofiz. Noveishie Tekhnol.) 42(4)
31. Belyansky M, Trenary M (1999) Comparison of the surface chemical reactivity of hafnium diboride and hafnium. Inorganica Chim Acta 289:191–197. https://doi.org/10.1016/S0020-1693(99)00068-7
32. Dikici B, Ozdemir I (2012) FeB and FeB/h-BN based anti-corrosive composite coatings for aluminium alloys. Anti-corros Methods M 59:246–254. https://doi.org/10.1108/00035591211265659
33. Dybkov V., "Basics of Formation of Iron Boride Coatings." *J. Miner.,***2** 30–46 (2016). 10.20941/2414–2115.2016.02.5.
34. Ivanovskii AL (2012) Mechanical and electronic properties of diborides of transition 3d–5d metals from first principles: toward search of novel ultra-incompressible and superhard materials. Prog Mater Sci 57:184–228. https://doi.org/10.1016/j.pmatsci.2011.05.004
35. Mayrhofer H, Stoiber M (2007) Thermal stability of superhard Ti–B–N coatings. Surf Coat Technol 201:6148–6153. https://doi.org/10.1016/j.surfcoat.2006.08.132
36. Mikula M, Grančič B, Roch T, Plecenik T, Vávra I, Dobročka E, Šatka A, Buršíková V, Držík M, Zahoran M, Plecenik A, Kúš P (2011) The influence of low-energy ion bombardment on the microstructure development and mechanical properties of TiBx coatings. Vacuum 85:866–870. https://doi.org/10.1016/j.vacuum.2010.12.011
37. Lofaj F, Moskalewicz T, Cempura G, Mikula M, Dusza J, Czyrska-Filemonowicz A (2013) Nanohardness and tribological properties of nc-TiB2 coatings. J Eur Ceram Soc 33:2347–2353. https://doi.org/10.1016/j.jeurceramsoc.2013.02.024
38. Rabinowicz E (1965) Friction and wear of materials. Wiley, New York

39. Akçamlı N, Ağaoğulları D, Balcı Ö, Öveçoğlu ML, Duman İ (2018) Room-temperature mechanochemical synthesis and consolidation of nanocrystalline HfB2-HfO2 composite powders. J Ceram Sci Technol 9:101–118. https://doi.org/10.4416/JCST2017-00084
40. Akçamlı N, Ağaoğulları D, Balcı Ö, Öveçoğlu ML, Duman İ (2017) Synthesis of bulk nanocrystalline HfB2 from HfCl4–NaBH4–Mg ternary system. J Mater Sci 52:12689–12705. https://doi.org/10.1007/s10853-017-1382-1
41. Novikov NV, Voronkin MA, Dub SN, Lupich IN, Malogolovets VG, Maslyuk BA, Podzyarey GA (1997) Transition from polymer-like to diamond-like a-C: H films structure and mechanical properties. Diamond Relat Mater 6:574–578. https://doi.org/10.1016/S0925-9635(96)00642-5
42. Leyland A, Matthews A (2000) On the significance of the H/E ratio in wear control: a nanocomposite coating approach to optimised tribological behaviour. Wear 246:1–11. https://doi.org/10.1016/S0043-1648(00)00488-9
43. Ni W, Cheng YT, Lukitsch MJ, Weiner AM, Lev LC, Grummon DS (2004) Effects of the ratio of hardness to Young's modulus on the friction and wear behavior of bilayer coatings. Appl Phys Lett 85:4028. https://doi.org/10.1063/1.1811377
44. Bhushan B (2017) Handbook of nanotechnology, fourth edition. Springer, Germany
45. Beake BD, Harris AJ, Liskiewicz TW (2013) Review of recent progress in nanoscratch testing. Tribol Mater Surf Interfaces 7:87–96. https://doi.org/10.1179/1751584X13Y.0000000037